

Resolving Interparticle Heterogeneities in Composition and Hydrogenation Performance between Individual Supported Silver on Silica Catalysts

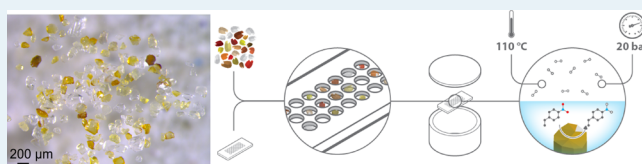
Eva Plessers,[†] Ivo Stassen,[†] Sreeprasant Pulinthanathu Sree,[†] Kris P. F. Janssen,[‡] Haifeng Yuan,[‡] Johan Martens,[†] Johan Hofkens,[‡] Dirk De Vos,[†] and Maarten B. J. Roeffaers^{*,†}

[†]Centre for Surface Chemistry and Catalysis, KU Leuven, Kasteelpark Arenberg 23, 3001 Heverlee, Belgium

[‡]Department of Chemistry, KU Leuven, Celestijnenlaan 200 F, 3001 Heverlee, Belgium

Supporting Information

ABSTRACT: Supported metal nanoparticle catalysts are commonly obtained through deposition of metal precursors onto the support using incipient wetness impregnation. Typically, empirical relations between metal nanoparticle structure and catalytic performance are inferred from ensemble averaged data in combination with high-resolution electron microscopy. This approach clearly underestimates the importance of heterogeneities present in a supported metal catalyst batch. Here we show for the first time how incipient wetness impregnation leads to 10-fold variations in silver loading between individual submillimeter-sized silica support granules. This heterogeneity has a profound impact on the catalytic performance, with 100-fold variations in hydrogenation performance at the same level. In a straightforward fashion, optical microscopy interlinks single support particle level catalytic measurements to structural and compositional information. These detailed correlations reveal the optimal silver loading. A thorough consideration of catalyst heterogeneity and the impact thereof on the catalytic performance is indispensable in the development of catalysts.



KEYWORDS: *interparticle heterogeneity, optical microscopy, selective catalytic hydrogenation, single-particle catalysis, supported metal catalysts*

INTRODUCTION

Supported platinum group metal (PGM) nanoparticles are heavily used as hydrogenation catalysts; however, their price and future availability call for alternatives. Even though silver is mostly known as an oxidation catalyst, e.g. in the industrial production of ethylene oxide and methanol, various research groups have shown that supported silver nanoparticles can also chemoselectively catalyze the hydrogenation of unsaturated aldehydes, esters, and nitro compounds;^{1–5} for the last example silver offers the unique possibility to chemoselectively reduce functional nitroaromatics to the corresponding anilines, which is not possible with PGM nanoparticles.^{6,7} The available information indicates that selective hydrogenation on supported silver catalysts is a structure-sensitive reaction in which, in addition to the structure of the substrate, also nanoparticle size and support material play an important role.^{1,2,8–10} In the selective hydrogenation of the unsaturated aldehydes crotonaldehyde and acrolein an increased reactivity and selectivity to the desired alcohol was found with increasing silver nanoparticle size.^{1,9} This observation was related to the larger fraction of Ag(111) surfaces. In contrast, smaller silver nanoparticles (0.9–3 nm) were found to be superior in the selective hydrogenation of 4-nitrostyrene¹¹ and acrolein¹² in the high-pressure range. These observations can be rationalized by the rate-limiting dissociation of H₂ at coordinatively unsaturated silver sites and the adsorption geometry of the

substrate. As often, these experimental results on the structure sensitivity of chemoselective hydrogenation with silver nanoparticles are seemingly contradictory, making clear-cut structure–activity assessments far from trivial. Supported-metal-catalyzed reactions are inherently chemically complex, and subtle changes in catalyst structure and properties can clearly have an important impact on the outcome.^{13,14} Rationalization of bulk catalytic performances, even when supported by molecular simulations, often oversimplify the inherent complexity of the supported metal catalyst itself.¹⁵ In addition to nanoparticle size and crystal facets also variations in loading, distribution, and accessibility could play an important role in the overall catalytic performance. Essential when experimentally establishing correct structure–activity relationships is the generation of nanoparticles of well-controlled sizes. However, it is known that common catalyst synthesis strategies preclude variability in nanoparticle size,^{16–18} making validation of the nanoparticle size indispensable. In addition to bulk techniques such as X-ray diffraction, chemisorption, and EXAFS that generally yield average nanoparticle diameters within a supported catalyst,⁹ direct imaging using transmission electron microscopy (TEM) allows precise determination of nanoparticle dimensions and dispersion.¹⁹ As a result of the

Received: September 22, 2015

Published: September 30, 2015

atomic resolution that can be achieved via TEM imaging, this approach is often the only suitable technique to study the size and dispersion of supported nanoparticles at the nanometer scale. Unfortunately, no direct link between these offline measurements and the catalytic performance can be made; thus, the catalytically active nanoparticles cannot be discriminated from spectator species.^{20,21}

In this study we report that typical incipient wetness impregnation results in an unexpected 10-fold variation in silver loading between individual silica gel support granules, leading to intersupport granule variations in number and size of the silver nanocatalysts. To validate the impact thereof on the catalytic performance, the selective reduction of 4-nitrostyrene to 4-vinylaniline was chosen. The aforementioned interparticle heterogeneity in silver loading leads to 100-fold variations in hydrogenation performance, and by using optical microscopy, it is possible to identify the optimal silver loading of the best-performing supported metal catalyst granules.

■ EXPERIMENTAL SECTION

Catalyst Preparation. An aqueous AgNO_3 solution, equaling the total pore volume of the support material, was added dropwise to dried silica gel (Sigma-Aldrich, Fluka 60752) until a slurry formed. After equilibration at room temperature the impregnated samples were dried overnight in air in an oven at 100 °C and finally calcined at 500 °C for 2 h. Control samples were obtained by calcining commercial AgNO_3 on silica gel (Sigma-Aldrich 248762) in air at 500 °C for 2 h. In this work this catalyst is referred to as “commercial Ag/SiO_2 ”.

Optical Microscopy. Images were obtained via the eyepieces using an adapter from Micro-Tech-Lab (Austria) to connect a Canon EOS5D color camera to an Olympus BX51 Upright microscope with a standard mercury lamp, equipped with infinity corrected air objectives 4× (0.16 N.A.) and 20× (0.40 N.A.). Color sorting of individual supported silver catalyst granules was performed on a stereomicroscope (Leica M165FC).

Scanning Electron Microscopy. High-resolution SEM images were obtained with a Nova NanoSEM 450 instrument (FEI). SEM-EDX was conducted using a FEI XL30FEG electron microscope equipped with an EDAX detector. Spectral analysis and quantification were performed with Genesis 4.61 software. Samples were mounted onto a copper TEM grid (300 mesh, Agar Scientific) fixed on a gold-coated cover slide which was then immobilized on to an aluminum stub using carbon sticker. These were imaged without any further sample modification.

Catalytic Performance Testing at the Bulk Level. Bulk hydrogenation reactions were performed in high-pressure 15 mL TOP reactors and a 100 mL Parr reactor (2 h, 110 °C, 20 bar of H_2 , 0.35 mol % of Ag, 70 mM 4-nitrostyrene in DMA, and 500 rpm unless stated otherwise). Analysis of the reaction products was carried out using a gas chromatograph (Shimadzu, CP-Sil 5, FID detector), and *n*-tetradecane was added as internal standard for quantitative GC analysis. Identification of the compounds was carried out using GC-MS.

Catalytic Performance Testing at the Single Support Particle Level. Individual single-granule hydrogenation reactions were performed by use of a multiwell placed in a 100 mL Parr reactor, enabling 21 reactions in parallel. Prior to the catalytic reaction, single support particles were carefully placed one by one in the different wells via an eyelash manipulator and a stereomicroscope (Leica M165FC). After

this, the multiwell could be filled with the reaction solution using a micropipette and placed in the reactor. Since thermal hydrogenation of 4-nitrostyrene results in the formation of the unwanted 4-ethylnitrobenzene and little 4-vinylaniline, in each run several wells were not filled with a catalyst particle to account for this blank conversion and some wells were only filled with solvent to ensure that no cross contamination had occurred. To lower solvent evaporation as much as possible, the high-boiling *N,N*-dimethylacetamide (DMA) was used as a solvent and *n*-hexadecane as an internal standard for quantitative GC analysis. Optimization of reaction conditions led to the use of 18 μL of a 33 mM 4-NSt solution in each microwell, with hydrogenation performed under 20 bar of H_2 on heating to 110 °C for 2.5 h in a Parr reactor filled with 3 mL of DMA. Analysis of the reaction products was carried out using a gas chromatograph (Shimadzu, CP-Sil 5, FID detector) after rinsing the wells two times with pure DMA.

■ RESULTS AND DISCUSSION

Compositional Heterogeneities at the Micro- and Nanoscale. Supported silver catalysts (5–6 wt % Ag) on silica gel were synthesized via standard incipient wetness impregnation.^{4,17} During calcination of the white silver nitrate impregnated silica powder, silver oxide was formed and subsequently at temperatures above 400 °C completely decomposed into metallic silver.^{22,23} The resulting silica-supported silver nanoparticle catalyst powder has a typical yellowish appearance and looks seemingly homogeneous. However, close inspection using optical microscopy revealed an unexpected variability in color between different support granules (Figure 1A–C); to our knowledge this interparticle

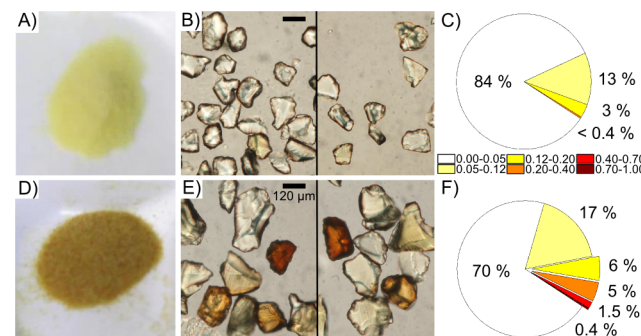


Figure 1. Interparticle heterogeneity in Ag/SiO_2 at the support granule level revealed by optical microscopy: (A–C) silver on silica gel obtained via typical incipient wetness impregnation; (D–F) commercial AgNO_3 on silica gel after calcination on the macroscale (A, D) and microscale (B, E) (C, F) Interparticle heterogeneity ($n = 250$) illustrated with pie diagrams. The colors represent the red color index of individual Ag/SiO_2 granules (for determination see the text in the Supporting Information and Figure S1).

color heterogeneity has not been reported so far for supported metal catalysts. An even more pronounced interparticle color heterogeneity, ranging from transparent to yellow to red-brown, was observed in a supported silver catalyst (6 wt % Ag) made by calcining commercial AgNO_3 on silica gel obtained from Sigma-Aldrich (Figure 1D–F). Strikingly, within one large support granule of about 100 μm in diameter no significant color variation was observed.

Since pure silica powder is optically transparent, also after a similar heat treatment, the observed color formation must be

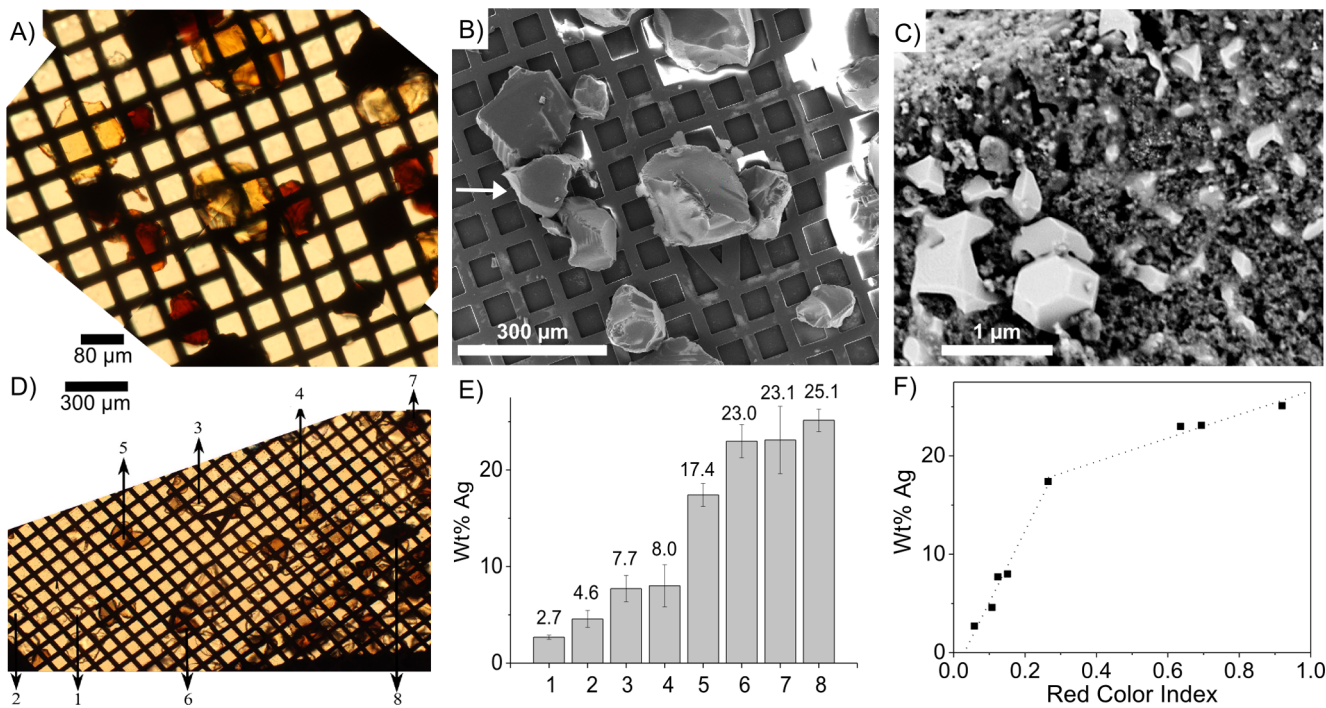


Figure 2. Correlation of the optical appearance of single Ag/SiO₂ granules to silver nanoparticle size (A–C) and silver loading (D–F). (A) Optical micrograph of single Ag/SiO₂ granules. (B) HR-SEM micrograph showing the overview of the same area. (C) HR-SEM micrograph of a dark support granule showing small nanoparticles (<10 nm, center) and very large silver nanoparticles (700–1000 nm, left lower corner). (D) Optical micrograph of single Ag/SiO₂ granules. (E) Silver loading of the numbered single Ag/SiO₂ granules measured via energy dispersive X-ray analysis. (F) Link between red color index of individual Ag/SiO₂ granules and their silver loading. The results shown here were obtained from the commercial 6 wt % Ag/SiO₂ catalyst.

associated with the silver nanoparticles. It is well-known that the optical appearance of silver nanoparticles is related to the surface plasmon resonance. Next to nanoparticle shape and refractive index of the environment, plasmon absorbance and hence selective (visible) light absorption is largely determined by the nanoparticle size.²⁴ For silver nanoparticles in silica below about 10 nm diameter the surface plasmon resonance peaks at around 420 nm, resulting in a yellow appearance upon white light illumination. Increasing the size to around 100 nm diameter results in a strong red shift of about 100 nm, which causes red coloration.²⁵ Nitrogen physisorption measurements of the used silica gel provide a BJH desorption average pore width of 60 Å (Figure S2 in the Supporting Information). Although the rather broad pore size distribution would give rise to polydisperse silver nanoparticles formed inside the support pores, their size is restricted to below 10 nm, resulting in an overall yellowish appearance. The presence of larger, unconfined silver nanoparticles at the outer surface of the support granules could give rise to color variations. However, several other factors will influence the optical appearance such as the local nanoparticle concentration and the absolute support granule size, which is directly linked to the optical path length and hence the resulting light absorption.²⁵ Since no relation was found between optical appearance and the absolute support granule size, the latter can be excluded and the color heterogeneity between individual silica granules must be sought at the level of the supported silver nanoparticles.

In order to investigate the color heterogeneity at the silver nanoparticle level, we resorted to high-resolution scanning electron microscopy (HR-SEM) correlated with optical microscopy. First, the optical appearance of the silica-supported silver catalyst was examined via optical microscopy after

deposition of the granules on a coverslip with a marked copper grid. Then, HR-SEM was performed to probe the outer surface of the same support granules, of which the optical color is known. Marks on the copper grid and the irregular shape of the support granules make the correlation of the optical images and SEM micrographs highly reliable (Figure 2A,B). By specific probing of the outer surface of transparent, yellow, and red granules, three distinct silver nanoparticle size ranges were noticed: 1–10, 20–50, and >400 nm (Figure S3 in the Supporting Information). The relative contribution of the larger 20–50 nm nanoparticles increases with increasing coloration, and the extremely large silver crystals (>400 nm) were only visible on the dark red silica granules (Figure 2C and Figure S3E). These electron micrographs thus evidence that there is a clear relation between color targeted via optical imaging and silver nanoparticle size at the outer surface of the support granules.

However, these findings do not exclude the possibility that the optical heterogeneity can also be induced by a difference in silver nanoparticle concentration, analogous to the observed heterogeneity in Pt/zeolite Y catalysts.¹⁹ Therefore, we adopted energy dispersive X-ray (EDX) spectroscopy to probe the silver content of individual silica support granules, again directly correlated to the optical appearance of the exact same granules (Figure 2D). Figure 2E shows that typical supported silver catalysts, obtained from a commercial supplier or via standard impregnation methods, display at least a 10-fold variation in silver loading between different silica support granules. Comparison of the EDX results and color indexing of the optical images led to a clear trend between optical appearance and silver content (Figure 2F). Since the silver content determined via SEM-EDX is limited to the first few

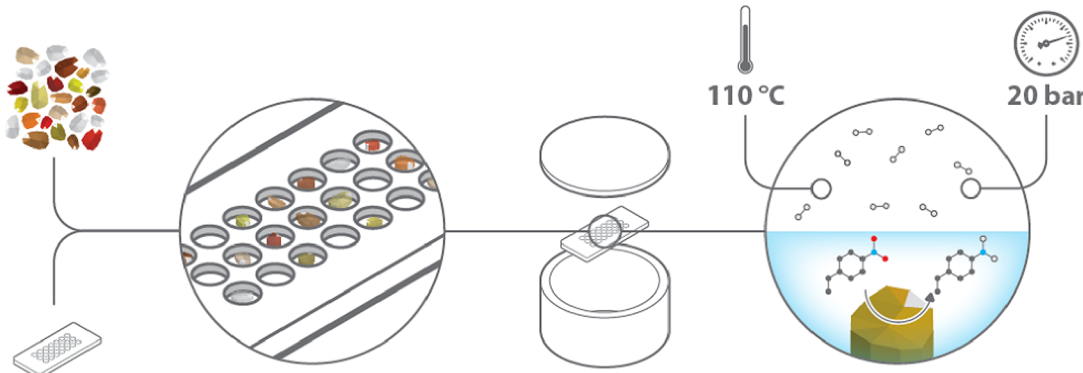


Figure 3. Schematic representation of a multiwell catalytic measurement at the single support particle level. In a typical run around 13 catalyst granules were tested together with four blank tests and two wells were only filled with solvent (18 μL of a 33 mM 4-NSt solution in each microwell, 20 bar of H_2 , 110 $^\circ\text{C}$, 2.5 h, 100 mL Parr reactor filled with 3 mL of DMA).

micrometers below the outer surface, this approach could lead to a misinterpretation of the total silver loading of this support granule because a silver gradient might exist along the cross section of the support granule.²⁶ To further validate the SEM-EDX measurements, focused ion beam (FIB) milling was used to section a yellow granule in the middle. A clear silver gradient can be observed, with silver concentrations decreasing from the outer surface of the granule toward the center; even in the center significant silver amounts could still be detected (Figure S4 in the Supporting Information). Furthermore, on these FIB sections no large silver nanoparticles were observed in the interior of the support granules with high-resolution SEM.

These correlated microscopy data link the optical appearance of a support granule to both silver concentration and size of nonpore confined silver nanoparticles at the outer surface. The increasing coloration observed in optical microscopy is related to both variations in silver loading and the presence of larger silver nanoparticles at the outer surface of the support granules. These calibration data can now be used to quantify the amount of silver in every support granule by simply using optical images. Optical microscopy is easily accessible without lengthy sample preparation and allows rapid determination of interparticle heterogeneity on the support granule level. Metal loading quantifications based on optical images rely on correlations with other analytical methods such as EDX, HR-SEM, etc.

Linking Hydrogenation Performance to Catalyst Composition via Catalytic Measurements at the Single Support Particle Level. Because of the large variability in silver loading and nanoparticle size it is not straightforward to unequivocally link performance to catalyst properties, certainly not from typical ensemble averaged measurements using at least milligrams of powdered catalyst. In this study we measured for the first time the catalytic performance at the level of the individual silica support granule. In order to minimize variations in experimental conditions, multiwell plates were used enabling 21 reactions in parallel in the same high-pressure Parr reactor; the multiwell catalytic measurements at the single support particle are shown schematically in Figure 3. These multiwell plates also allow recording of optical transmission images of the individual supported catalyst granules placed in each reaction well; from these optical images the exact silver content in every microwell is determined, which is critical for normalizing catalyst performance. Subsequently, after 590 nmol of 4-nitrostyrene (4-NSt)

in 18 μL of *N,N*-dimethylacetamide (DMA) solvent was added, the multiwell plate was loaded in the Parr hydrogenation reactor at 20 bar of H_2 and heated to 110 $^\circ\text{C}$; under these conditions no distillation of the reactant or its products was observed. After 2.5 h the reaction mixture of every microwell was analyzed via gas chromatography. Figure 4A shows the normalized catalytic performance of 47 individual supported catalyst granules as a function of their total silver loading (more details are given in the Supporting Information).

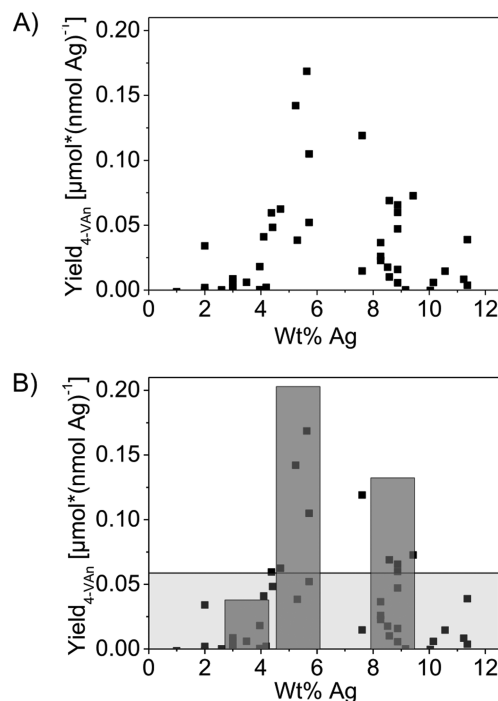


Figure 4. (A) Single-granule catalytic hydrogenation of 4-nitrostyrene with commercial Ag/SiO_2 catalyst: results of 47 individual silver supported silica granules. Estimation of silver loading was based on red color index and SEM-EDX, complemented by ICP-AES measurements of color-sorted granules. More details can be found in the text and Figure S5 of the Supporting Information. (B) Bulk hydrogenation reactions with color-sorted commercial Ag/SiO_2 samples (column bars), displaying up to a 2.5-fold increase of yield with respect to unsorted commercial catalyst (filled area) (110 $^\circ\text{C}$, 20 bar of H_2 , 2.5 h).

These single support particle data undoubtedly reveal an optimal silver loading. Granules with about 6 wt % of silver show up to 100-fold higher normalized 4-vinylaniline yield in comparison to catalyst granules from the same batch containing <4 wt % or >8 wt % of silver. From the detailed physicochemical characterization (*vide supra*) the highest hydrogenation performance can be attributed to support granules with yellow appearance (red color index 0.12–0.20): i.e., 5–7 wt % silver. These yellow granules contain in addition to the 6 nm pore confined silver nanoparticles also a reasonable amount of larger, 20–50 nm silver nanoparticles on the surface of the support granule. When a whole support granule is considered, the pore confined silver nanoparticles represent over 99.9% of the total number of nanoparticles. Silver in these yellow granules is up to 100 times more efficiently used as in highly loaded (>8 wt % Ag) support granules, with silver nanoparticles larger than 400 nm on the support's outer surface, and as in transparent granules (<4 wt % Ag) which only contain the pore confined 6 nm silver nanoparticles. Hence, it can be concluded that in this sample support granules with 6 wt % silver and the highest relative contribution of 20–50 nm silver nanoparticles are the most active in the selective 4-nitrostyrene reduction, contradicting earlier reports based on ensemble-averaged hydrogenation data.¹¹

Rationally Improving the Hydrogenation Performance of Supported Silver Catalysts. In order to validate these single support particle results, namely that the catalyst granule's optical appearance is linked to the silver content and its catalytic performance, we carried out bulk catalytic hydrogenation reactions. Ag/SiO₂ samples with four different silver contents ranging from 4 to 19 wt % at the bulk level were synthesized. As expected, all of these materials showed a significant interparticle heterogeneity in optical appearance (*Figure S6* in the Supporting Information). Using the average performance determined for every color of catalyst granule via single support particle experiments, the estimated theoretical 4-vinylaniline yield of each of these catalyst samples was estimated (*Figure 5*; the calculation is explained in the Supporting Information). These calculations predict that the sample with a bulk loading of 13 wt % in silver should show the best selective hydrogenation performance. Indeed, in a typical hydrogenation reaction with 0.35 mol % silver and with the same relative amounts of substrate and solvent as were used in

the multiwell experiments, a similar performance trend was observed (*Figure 5*). In addition, the results of the commercial Ag/SiO₂ sample (6 wt %) fit perfectly within the results of the self-synthesized samples. The outcome of the single support particle experiments can thus undoubtedly be extrapolated to the bulk level. Although the normalized yield of the commercial sample increased by 38% upon increasing the overall silver loading to 13 wt %, a considerably higher improvement must be possible on the basis of the observed heterogeneity. Ideally one would rationally synthesize a batch which consists of only yellow supported silver catalyst granules; however, none of the typical impregnation approaches gave a satisfactory result. In an attempt to obtain a more homogeneous catalyst sample, the commercial silver on silica catalyst was manually sorted into three different fractions (*Figure S7* in the Supporting Information). As can be expected from the single support particle experiments, the batch with yellow support granules outperforms the batches with transparent or orange and red granules to the same degree as could be expected from the single support particle studies (*Figure 4B*).

CONCLUSIONS

We have shown that typical incipient wetness impregnation brings about severe heterogeneity in metal loading at the support particle level. Specifically, 10-fold variations in silver metal loading between individual silica support granules are no exception within one catalyst batch. These differences in metal loading severely affect the catalytic performance on measurement at the same scale. Here optical microscopy proved to be a convenient tool to directly interlink the physicochemical properties and hydrogenation performance of individual support particles. Following this approach, we could resolve 100-fold variations in normalized catalytic performance for the selective 4-nitrostyrene reduction and determine the optimal silver loading for this reaction. More specifically, these single-particle experiments indicate that support granules which have the relative highest contribution of silver nanoparticles of about 20–50 nm show the highest 4-vinylaniline (4-VAn) yield. Following traditional catalyst impregnation optimization based on ensemble averaged characterization and catalytic performance measurements it would be far from trivial to find this optimal catalyst composition. The proposed optical screening method is widely applicable to supported metal catalysts: e.g., similar heterogeneity in color and thus loading were also observed in Pt/SiO₂ (*Figure S8* in the Supporting Information).

ASSOCIATED CONTENT

Supporting Information

The Supporting Information is available free of charge on the ACS Publications website at DOI: 10.1021/acscatal.5b02119.

Additional information regarding the experimental execution and data analysis and FIB-SEM, N₂-physisorption, and Pt/SiO₂ data ([PDF](#))

AUTHOR INFORMATION

Corresponding Author

*E-mail for M.B.J.R.: maarten.roeffaers@biw.kuleuven.be.

Notes

The authors declare no competing financial interest.

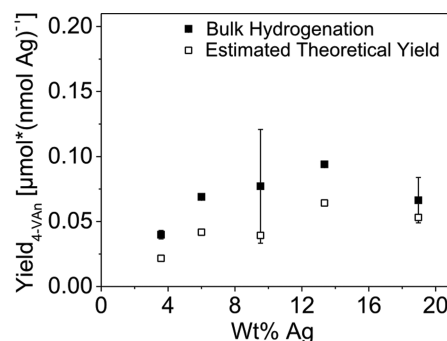


Figure 5. Bulk hydrogenation reactions of 4-nitrostyrene with self-synthesized (4 to 10, 13, and 19 wt % Ag) and commercial 6 wt % Ag/SiO₂ catalysts (■) and estimated theoretical yield based on optical appearance (□) (for the determination see the Supporting Information, silver loading based on ICP-AES) (110 °C, 20 bar of H₂, 2 h).

■ ACKNOWLEDGMENTS

The authors thank the Research Foundation-Flanders (FWO) (Grant G.0990.11 and G.0962.13, Ph.D. scholarships to E.P. and I.S. and postdoctoral fellowships to K.P.F.J. and H.Y.), Belspo (IAP-VII/05), and the Flemish government (Long term structural funding-Methusalem funding CASAS METH/08/04). M.B.J.R. acknowledges the European Research Council for financial support (ERC Starting Grant LIGHT 307523).

■ REFERENCES

- (1) Wei, H.; Gomez, C.; Liu, J.; Guo, N.; Wu, T.; Lobo, R.; Christopher, L.; Lobo-Lapidus, R.; Marshall, C. L.; Miller, J. T.; Meyer, R. J. *J. Catal.* **2013**, *298*, 18.
- (2) Shimizu, K.; Sawabe, K.; Satsuma, A. *Catal. Sci. Technol.* **2011**, *1*, 331.
- (3) Yin, A.; Guo, X.; Dai, W.; Fan, K. *Chem. Commun.* **2010**, *46*, 4348.
- (4) Steffan, M.; Jakob, a; Claus, P.; Lang, H. *Catal. Commun.* **2009**, *10*, 437.
- (5) Chen, Y.; Wang, C.; Liu, H.; Bao, X.; Qiu, J. *Chem. Commun.* **2005**, *2*, 5298.
- (6) Corma, A.; Serna, P. *Science* **2006**, *313*, 332.
- (7) Furukawa, S.; Yoshida, Y.; Komatsu, T. *ACS Catal.* **2014**, *4*, 1441.
- (8) Corain, B.; Schmid, G.; Toshima, N. *Metal Nanoclusters in Catalysis and Materials Science: The Issue of Size Control*; Elsevier: Amsterdam, 2007; Chapter 8.
- (9) Claus, P.; Hofmeister, H. *J. Phys. Chem. B* **1999**, *103*, 2766.
- (10) Hirunsit, P.; Shimizu, K.; Fukuda, R.; Namuangruk, S.; Morikawa, Y.; Ehara, M. *J. Phys. Chem. C* **2014**, *118*, 7996.
- (11) Shimizu, K.; Miyamoto, Y.; Satsuma, A. *J. Catal.* **2010**, *270*, 86.
- (12) Bron, M.; Teschner, D.; Knopgericke, a; Steinhauer, B.; Scheybal, A.; Havecker, M.; Wang, D.; Fodisch, R.; Honicke, D.; Wootsch, A. *J. Catal.* **2005**, *234*, 37.
- (13) De Jong, K. P. *Synthesis of Solid Catalysts*; Wiley-VCH: Weinheim, Germany, 2009; Chapters 1–5.
- (14) Morbidelli, M.; Gavriilidis, A.; Varma, A. *Catalyst Design: Optimal Distribution of Catalyst in Pellets, Reactors, and Membranes*; Cambridge University Press: Cambridge, U.K., 2001; Chapter 7.
- (15) Gao, F.; Goodman, D. W. *Annu. Rev. Phys. Chem.* **2012**, *63*, 265.
- (16) Ertl, G.; Knözinger, H.; Schüth, F.; Weitkamp, J. *Handbook of Heterogeneous Catalysis*; Wiley-VCH: Weinheim, Germany, 2008; Chapter 2.
- (17) White, R. J.; Luque, R.; Budarin, V. L.; Clark, J. H.; Macquarrie, D. J. *Chem. Soc. Rev.* **2009**, *38*, 481.
- (18) Prieto, G.; Friedrich, H.; De Jong, K. P.; De Jongh, P. E.; Zečević, J.; de Jong, K. P.; de Jongh, P. E. *Nat. Mater.* **2012**, *12*, 34.
- (19) Zečević, J.; van der Eerden, A. M. J.; Friedrich, H.; de Jongh, P. E.; de Jong, K. P. *ACS Nano* **2013**, *7*, 3698.
- (20) Sambur, J. B.; Chen, P. *Annu. Rev. Phys. Chem.* **2014**, *65*, 395.
- (21) Niemantsverdriet, J. W. *Spectroscopy in Catalysis*; Wiley-VCH: Weinheim, Germany, 2007; p 325.
- (22) Waterhouse, G. I. N.; Bowmaker, G. a.; Metson, J. B. *Phys. Chem. Chem. Phys.* **2001**, *3*, 3838.
- (23) Weaver, J. F.; Hoflund, G. B. *J. Phys. Chem.* **1994**, *98*, 8519.
- (24) Sun, Y.; Xia, Y. *Analyst* **2003**, *128*, 686.
- (25) Quinten, M. *Appl. Phys. B: Lasers Opt.* **2001**, *73*, 317.
- (26) Espinosa-Alonso, L.; Beale, A. M.; Weckhuysen, B. M. *Acc. Chem. Res.* **2010**, *43*, 1279.